Eur. Phys. J. E (2018) **41**: 73
DOI 10.1140/epje/i2018-11684-9

THE EUROPEAN PHYSICAL JOURNAL E

Regular Article

Dislocations dynamics during the nonlinear creep of a homeotropic sample of smectic-A liquid crystal

P. Oswald[a] and G. Poy

Univ Lyon, ENS de Lyon, Univ Claude Bernard, CNRS, Laboratoire de Physique, F-69342 Lyon, France

Received 27 April 2018 and Received in final form 25 May 2018
Published online: 12 June 2018

Abstract. New creep experiments under sinusoidal compression/dilation deformation of a homeotropic sample of smectic-A liquid crystal (8CB) show that its response is nonlinear at very small amplitude of deformation. This behavior is explained by taking into account the crossing between the edge dislocations that climb parallel to the layers and the screw dislocations joining the two surfaces limiting the sample. The activation energy of the crossing process and the density of the screw dislocations as a function of the sample thickness are estimated experimentally.

1 Introduction

A smectic-A liquid crystal (SmA-LC) is a lamellar phase with fluid layers and the rod-shaped molecules perpendicular to the layers [1]. At equilibrium the layers are planar and spaced by the equilibrium period b_0. Because of its structure, a SmA behaves as a solid under compression/dilation normal to the layers and as a liquid under shear. The solid behavior was evidenced experimentally for the first time by Bartolino and Durand in 1977 [2]. In their experiment, a homeotropic sample was compressed normal to the layers. The deformation was extremely small (less than 10^{-5}) and was produced by a piezoelectric ceramic. With this system, these authors directly measured the compression modulus B of the layers and detected the plastic relaxation of the applied stress. This relaxation was attributed to the climb motion of the edge dislocations always present in the homeotropic samples because of the angle α —never equal to zero— between the two glass plates limiting the sample. A remarkable point is that only the geometrical dislocations survive in well-annealed homeotropic samples. For this reason, they form at mid-distance of the glass plates a subgrain boundary with an average distance between them $\Lambda = b/\alpha$ as illustrated in fig. 1. This was shown by direct visualization of the dislocations under the optical microscope. Two methods were used to see them: the first one was known for a long time and consists of working at the smectic-A–smectic-C phase transition temperature [3]. At this temperature, the SmC phase (in which the molecules are tilted with respect to the normal to the layers) first develops near the core of the dislocations which thus become visible between crossed polarizers. A second method, more recent, consisted of doping the SmA-LC with nanoparticles [4]. In that case, Cottrell clouds [5,6] form around the core of the dislocations which becomes visible at all temperatures under the microscope.

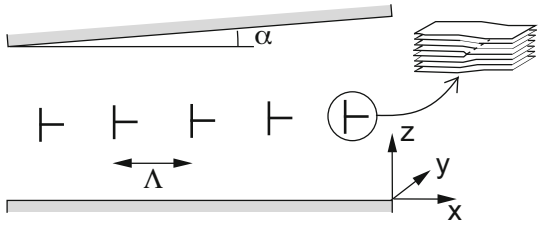

Fig. 1. Schematic representation of the subgrain boundary formed by the geometrical edge dislocations present in the sample.

Edge dislocations are not the only defects present in homeotropic samples. There also exists a large density of screw dislocations (presumably elementary because of the quadratic dependence of their energy with respect to their Burgers vector [7]). These defects are usually invisible under the polarizing microscope in samples of SmA-LC but can be seen in SmC*-LC under crossed polarizers (see, for instance, refs. [8,9]). In SmA-LC, screw dislocations were first evidenced in lyotropic systems by observing in TEM (transmission electron microscopy) the replica of the surface of frozen samples cleaved parallel to the layers [10,11].

[a] e-mail: patrick.oswald@ens-lyon.fr

These defects were also observed by confocal microscopy in SmA samples frozen in liquid nitrogen [12]. There also exist indirect evidence of these defects in microplasticity, when a homeotropic sample is submitted to a large deformation (up to 10^{-3} under compression normal to the layers). Such a deformation can be reached by stacking several tens of piezoelectric ceramics as in the rheometer used for this study (for a description, see [13]). In this case, the experiment shows that the stress relaxes faster at large deformation than at small one. More precisely, the stress relaxation time decreases by successive jumps when the stress increases, revealing an original sequence of helical instabilities of the screw dislocations present in the samples [14]. This instability was first observed in a thick sample ($400\,\mu$m thick) [15] and later in samples a few micrometers thick by using a force machine [16].

Most of the plasticity experiments mentioned above were performed with the LC 8CB (4-*n*-octylcyanobiphenyl). In this LC, the interactions between the edge dislocations and screw dislocations were neglected so far, in particular when they intersect. The main reason for this is that the energy of the kink formed on the edge dislocation during the crossing is expected to be very small because of its screw character (the energy of a screw dislocation is very small in SmA-LC, probably ten times smaller than that of an edge dislocation [7]). This hypothesis seems nevertheless questionable in view of more recent experiments performed by Lelidis and coworkers in another material exhibiting a SmA-to-SmC phase transition [17–19]. In this material, these authors observed that, at small deformations, the edge dislocations are pinned on localized obstacles that they suspected to be screw dislocations. This hypothesis was reinforced by the calculation in covariant elasticity of the elastic force between an edge and a screw dislocation.

For this reason, we reconsidered this question of the crossing between edge and screw dislocations in the LC 8CB by performing new microplasticity experiments at very small amplitude of deformation. In this regime, the interaction must be visible if it exists.

The plan of the paper is as follows. In sect. 2, we present the piezoelectric rheometer, its equivalent mechanical model and its calibration with a known silicon oil. Section 3 is devoted to the measurements of the elastic constants and the mobility of edge dislocations in the 8CB LC at large amplitude of deformation. We show that the simplified metallurgical model used so far (in particular in [5]), which neglects the interaction between edge and screw dislocations, works in this regime. In sect. 4, we study the rheological behavior of the sample when the amplitude of deformation is decreased. We show that the apparent viscosity of the sample increases when the amplitude of deformation decreases, in contradiction with the simplified model. To explain this nonlinear behavior, we propose a new metallurgical model taking into account the presence of obstacles disturbing the motion of the edge dislocations. The nature of these obstacles is then discussed in view of our experimental results. Conclusions are drawn in sect. 5.

2 The piezoelectric rheometer: equivalent model and calibration

The piezoelectric rheometer used for this study is described in ref. [13]. Several improvements have been made. The first one is a locking system for each of the differential screws used to change the thickness of the sample. Thanks to this new system, the rheometer is more rigid and less sensitive to mishandling. Another improvement (already used in ref. [20]) is that the two ovens are now controlled in temperature independently of each other to within $0.01\,^{\circ}$C thanks to two RKC HA400 controllers. The rheometer and its microscope are also inside a plexiglass box regulated at $22 \pm 0.1\,^{\circ}$C. This is important to improve the mechanical stability of the rheometer during the measurements, in particular at low deformation (thickness variations of the order of the layer thickness) and low frequency (down to 10^{-2} Hz). In addition, each oven is now closed with a sapphire window in order to decrease the thermal gradient inside the sample. With this new protection, the temperature is homogeneous to within $\pm 0.02\,^{\circ}$C over the whole surface of the sample. Circular 3 mm thick $\lambda/4$ glass plates from Edmund Optics are used to prepare the sample. The upper plate has a diameter of 10 mm and the bottom one a diameter of 12.5 mm. Both are treated for homeotropic anchoring with the Merck silane ZLI 3124. The solvent used to dissolve the silane is a 2:1 mixture of toluene and dichloromethane. In practice the glass plates are dipped in the silane solution and then rapidly removed in order that the solution dewets the surface. If traces of silane remain on the glass, they are removed by gently polishing the surface with an optical paper. The process is then repeated until the glass dewets perfectly. In this way a very strong homeotropic anchoring is achieved. The initial thickness of the sample and the angle α between the two glass plates are measured before filling with a fibre optic spectrometer (USB 650-Ocean Optics). The former is known to within $\pm 0.2\,\mu$m and the second to within $\pm 10^{-5}$ rad. Once the cell is filled with the LC, the thickness and the angle can be changed independently thanks to the three differential screws and the ATA 101 Schaevitz LVDT sensor used to measure the thickness variation of the sample. A lock-in amplifier Stanford SR850 is used to excite the ceramics and measure the sample deformation and its phase shift with respect to the excitation. Finally, a Labview program allows one to control the lock-in amplifier and the two temperature controllers and to generate automatic ramps of amplitude (frequency) at fixed frequency (amplitude). Note that between each ramp of amplitude or frequency, the sample is melted in the nematic phase. This is important, in particular when the microstructure of the sample changes, which may happen in some of our experiments in which the onset of the undulation instability of the layers is overcome. The sample is then cooled down to the temperature chosen for the measurement. The cooling must be very slow (in practice we choose $-0.1\,^{\circ}$C/min) because the sample slightly dilates by about $0.2\,\mu$m/$^{\circ}$C when it is cooled down. This precaution is essential to avoid the undulation instability of the layers and the nucleation of

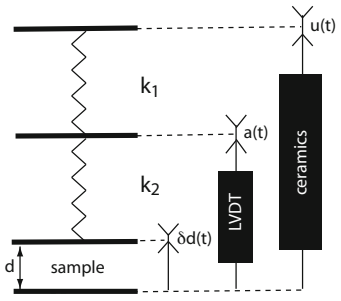

Fig. 2. Equivalent mechanical model of the rheometer.

focal parabolas which would change the microstructure of the sample.

From a mechanical point of view, the rheometer can be modeled by two springs of force constants k_1 and k_2 in series with the sample (fig. 2). In practice, the displacement $u(t)$ is imposed by three stacks of piezoelectric ceramics and the displacement $a(t)$ is measured with the Schaevitz sensor. The displacements $u(t)$ and $a(t)$ (rigorously, its first harmonic) and their phase shift Φ are measured with the lock-in amplifier when a sinusoidal deformation is imposed to the sample. In this case, $u(t) = u_0 \sin(\omega t)$ and $a(t) = a_0 \sin(\omega t + \Phi)$, with $u_0 \approx 20\,\text{nm}$ when a sinusoidal voltage V of 1 Vrms is applied to the ceramics.

To measure the two constants k_1 and k_2, we used the silicon oil 47V10000 (Bluestar silicones). At low frequency (in the terminal regime), this oil behaves as a Maxwell fluid of viscosity η and elastic modulus G (with $\tau = \eta/G$ the viscoelastic relaxation time). In this case, the motion equations read

$$\sigma = k_1(u - a) = k_2(a - \delta d), \tag{1}$$

$$\sigma = \frac{3}{2}\frac{R^2}{d^2}\left(\frac{G''}{\omega}\frac{\dot{\delta d}}{d} + G'\frac{\delta d}{d}\right), \tag{2}$$

where G' and G'' are the elastic and loss moduli:

$$\begin{cases} G' = \dfrac{\eta\tau\omega^2}{1+\omega^2\tau^2}\,, \\ G'' = \dfrac{\eta\omega}{1+\omega^2\tau^2}\,. \end{cases} \tag{3}$$

Solving these equations gives the amplitude ratio a_0/u_0 and the phase shift Φ [20]:

$$\begin{cases} \dfrac{a_0}{u_0} = \sqrt{\dfrac{(1+\beta C)^2\omega_r^2 + C^2\omega^2}{(1+\beta+\beta C)^2\omega_r^2 + (1+C)^2\omega^2}}\,, \\ \tan(\Phi) = -\dfrac{\omega\omega_r}{(1+\beta C)(1+\beta+\beta C)\omega_r^2 + C(1+C)\omega^2}\,, \end{cases} \tag{4}$$

where $C = k_1/k_2$ and

$$\beta = \frac{3R^2}{2k_1d^3}G', \tag{5}$$

$$\omega_r = \frac{2k_1d^3}{3R^2}\frac{\omega}{G''}\,. \tag{6}$$

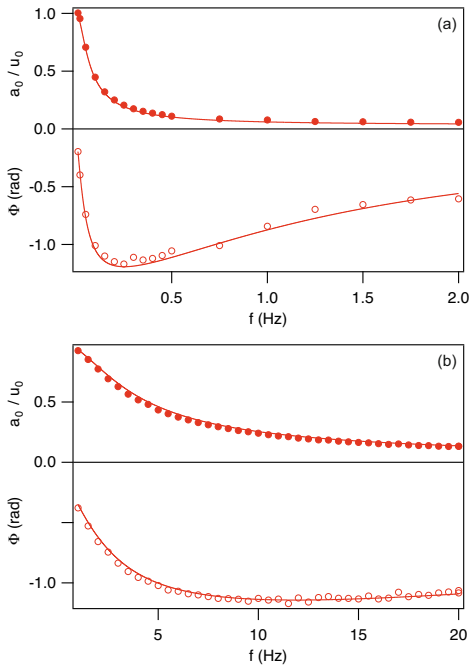

Fig. 3. Rheological curves measured at 25 °C with the silicon oil 47V10000 at $d = 103\,\mu$m and $d = 23\,\mu$m. The solid lines show the best fits with the model.

These formulae can be used to fit the experimental data obtained with the silicon oil. In practice, we measured the experimental curves $a_0/u_0(f)$ and $\Phi(f)$ (with $\omega = 2\pi f$) at three different thicknesses: $d = 27, 53$ and $103\,\mu$m, and we then fitted together the six curves obtained by taking k_1, C and τ as fit parameters with $\eta = 100\,\text{P}$. This procedure led to $C = 0.038$, $k_1 = 4.22\ 10^8\,\text{dyn/cm}^3$ and $\tau = 4.4\ 10^{-3}\,\text{s}$. This value of τ is in very good agreement with the fact that this oil becomes shear-thinning above a typical shear rate of $200\,\text{s}^{-1}$, which is indeed very close to $1/\tau$. An example of experimental curves is shown with its fit in fig. 3.

In the next two sections, we present our experimental results obtained with the LC 8CB (from Frinton Laboratories, USA). For this LC we measured $T_{NA} = 33.33\,^\circ\text{C}$. All of our experiments were performed at $T = 32.00\,^\circ\text{C}$ with an angle $\alpha = 10^{-3}\,\text{rad}$. This angle was chosen twice larger than in our previous work [5].

3 Microplasticity at large deformation

In this section, we restrict ourselves to the large-amplitude regime in which the interactions between the edge and screw dislocations can be neglected. The amplitude of deformation must nevertheless be not too large to avoid both the helical instabilities of the screw dislocations and the undulation instability of the layers [21] rapidly followed by the nucleation of focal parabolas [22]. If these conditions are fulfilled, the microstructure of the sample remains unchanged during the experiments (no nucleation of new dislocations) and the curves measured at

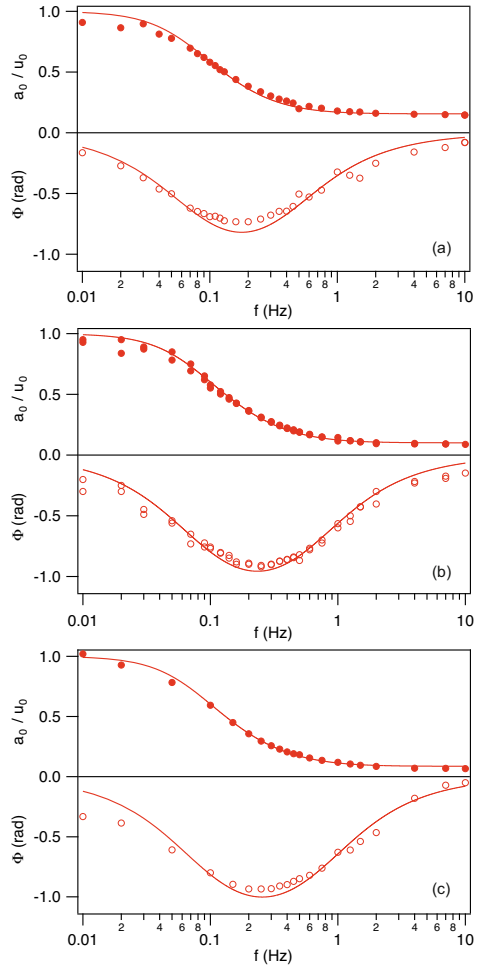

Fig. 4. Three examples of curves measured in the large-deformation regime. In (a) $d = 50\,\mu$m and $V = 9$ Vrms ($u_0 \approx 180$ nm); in (b) $d = 100\,\mu$m and $V = 5$ Vrms ($u_0 \approx 100$ nm); in (c) $d = 200\,\mu$m and $V = 2.25$ Vrms ($u_0 \approx 45$ nm). Note that the curves in (c) have been measured at both decreasing and increasing frequencies. The solid lines are the best fits with the simplified model neglecting the interactions with the screw dislocations.

increasing frequency must perfectly superimpose with the curves measured at decreasing frequency. In practice, we determined that the maximum operable voltage satisfying this criterion is close to 9 Vrms at 50 μm, 5 Vrms at 100 μm and 2.25 Vrms at 200 μm. Three curves measured at these thicknesses and these voltages are shown in fig. 4. Note that in fig. 4(b), the points measured at increasing frequency superimpose with those found at decreasing frequency.

To model these curves, we assume that the stress relaxes inside the sample because of the climb of the edge dislocations. In this model, each dislocation moves at velocity $v = m\sigma$, where m is its mobility. Let x be the distance covered by each dislocation at time t. Because of the motion of the dislocations, the stress σ relaxes and is given by

$$\sigma = B\frac{\delta d}{d} - B\frac{\alpha x}{d}\,. \tag{7}$$

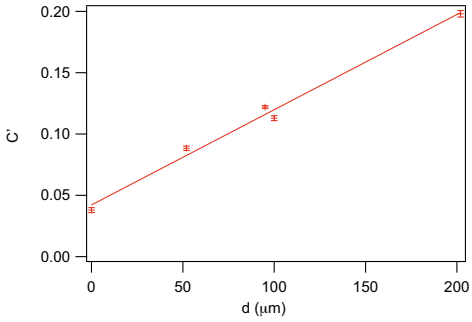

Fig. 5. Constant C' as a function of the thickness d. The value reported at $d = 0$ is the value of C measured with the silicon oil. The other points are averages over several measurements in the large-amplitude regime. The solid line is a linear fit.

Knowing that $v = \mathrm{d}x/\mathrm{d}t = m\sigma$, we obtain after elimination of x from eqs. (1) and (7):

$$\omega_c(u - a) = (1 + C')\frac{\mathrm{d}a}{\mathrm{d}t} - C'\frac{\mathrm{d}u}{\mathrm{d}t}\,, \tag{8}$$

where $\omega_c = 2\pi f_c = k_1 m\alpha$ is a stress relaxation frequency independent of the thickness and $C' = C + k_1 d/B$. Solving the previous equation for a sinusoidal deformation yields

$$\begin{cases} \dfrac{a_0}{u_0} = \sqrt{\dfrac{\omega_c^2 + C'^2\omega^2}{\omega_c^2 + (1 + C')^2\omega^2}}\,, \\ \tan(\Phi) = -\dfrac{\omega\omega_c}{\omega_c^2 + C'(1 + C')\omega^2}\,. \end{cases} \tag{9}$$

The best fit of the experimental curves of fig. 4 gives $C' = 0.184$ and $f_c = 0.082$ Hz for $d = 200\,\mu$m, $C' = 0.11$ and $f_c = 0.082$ Hz for $d = 100\,\mu$m and $C' = 0.095$ and $f_c = 0.079$ Hz for $d = 50\,\mu$m. In agreement with the model, f_c does not depend on the thickness while C' increases linearly with the thickness (fig. 5). From the value of f_c and the slope of the curve $C'(d)$ we calculate $m = 1.2\ 10^{-6}$ cm/P and $B = 5.4\ 10^7$ dyn/cm^2. These two values are in excellent agreement with the values given in ref. [5] at the same temperature, but measured with an angle α twice as small. This good agreement at two different angles proves once again that the geometrical edge dislocations are well responsible for the relaxation of the elastic stress and that the simplified model neglecting the interactions with the screw dislocations can be used in the large-amplitude regime. We also emphasize that the mobility found here is in excellent agreement with the value of the mobility obtained from the direct observation of the dislocation dynamics in thick free-standing films [23–25].

To complete these measurements, we measured the penetration length $\lambda = \sqrt{K/B}$, where K is the curvature modulus of the layers. The measurement was done at 10 Hz. At this frequency, the dislocations are almost "frozen" and contribute very little to the deformation of the sample. Figure 6 shows the ratio a_0/u_0 as a function of the maximum stress σ_{max} that the sample experiences during the oscillations. This stress is calculated from the

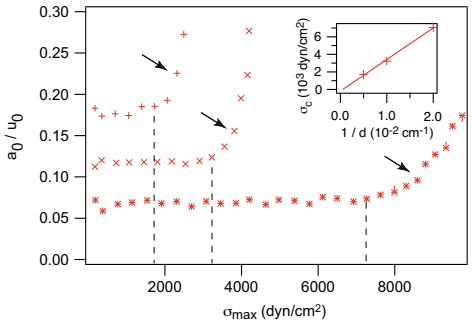

Fig. 6. Ratio a_0/u_0 as a function of the maximal stress σ_{max} imposed to the sample. The sample thickness is $d = 200\,\mu$m (+), $d = 200\,\mu$m (×) and $d = 50\,\mu$m (∗). The vertical bars mark the onset of the undulation instability (σ_c). The arrows indicate when the focal parabolas become visible in the sample. Inset: critical stress σ_c as a function of $1/d$.

formula

$$\sigma_{max} = k_1 a_0 \sqrt{1 + \frac{u_0^2}{a_0^2} - 2\cos\Phi\frac{u_0}{a_0}}\,. \tag{10}$$

For each thickness there exists a stress σ_c below which the ratio a_0/u_0 is constant and above which it increases. This increase is due to the undulation instability of the layers and the nucleation of focal parabolas in the sample [22] (the arrows in the figure mark at which stresses the focal parabolas become visible in the microscope). In the inset, the stress σ_c is plotted as a function of the reciprocal of the thickness $1/d$. As expected, σ_c is inversely proportional to d in agreement with the calculation of the onset of instability which gives $\sigma_c = 2\pi B\lambda/d$ [21]. From the slope of the curve and the value of B given above we deduce $\lambda = 1.0\,$nm and $K = 5.4\ 10^{-7}\,$dyn. This value is again in good agreement with our previous measurements [26].

4 Microplasticity at small deformation

4.1 Experimental results

Thanks to the improvements made to our rheometer, we were able to explore the plastic behavior of the smectic phase at smaller deformations than in our previous experiments. Doing this, we realized that the apparent sample viscosity increases when the amplitude of deformation decreases. This can be seen in fig. 7 showing typical rheological curves measured at different voltages and thicknesses. These graphs show that the response of the smectic changes when the amplitude of deformation decreases, which is in contradiction with the previous linear model. More precisely, the smaller the thickness, the faster the curves $a_0/u_0(f)$ decreases when f increases, while the minimum of the curves $\Phi(f)$ shifts toward the low frequencies. This is a clear indication of an hardening of the sample. A good way of quantifying this effect is to fit the curves with eqs. (9) of the simplified model. Surprisingly, the fits remain correct at all frequencies and lead to unchanged values of C' (fig. 8(a)) whereas the values of f_c decrease when the amplitude of deformation decreases while saturating towards a single value (independent of the thickness) at large amplitude (fig. 8(b)) (as predicted by the simplified model). The fact that the measured elastic modulus does not change even at very small amplitude of deformation and that the curves can still be fitted with the simplified model at low frequency clearly indicates that the edge dislocations in 8CB are not strongly pinned on obstacles as in the experiments of Lelidis *et al.* [12, 17–19]. This is also compatible with our direct observations of the edge dislocations when they are decorated with gold nanoparticles [5] and move slowly under the action of a temperature change. On the other hand, the fact that f_c decreases at small amplitude clearly indicates that their mobility decreases, which means that obstacles disturb their motion. As there is no measurable yield stress in our system, we must assume that these obstacles can be overcome by thermal activation. This led us to develop the following model.

4.2 Dislocation mobility in the presence of obstacles

To calculate the average mobility of the dislocations, we suppose that each dislocation is held up by a forest of obstacles of size h at average distance L apart. In other words, $1/L^2$ is the number of obstacles per unit surface area in the plane of the sample. Let ΔE be the energy required to cause the dislocation to cross an obstacle. During the crossing, the dislocation line sweeps out an area Dh and the applied stress does work $Dhb\sigma$ by denoting by D the average distance between the obstacles along the line (fig. 9). This distance D can be calculated. Two regimes must be considered: the low-stress regime in which D varies as $1/\sigma^{1/3}$ as shown by Friedel [27] and the large-stress regime in which $D = L$ as shown numerically by Foreman *et al.* [28]. We will show later that, in our experiments, we are always in the limit $D = L$. For this reason and to simplify the discussion, we will assume from now on that $D = L$. This results in an activation energy $U^+ = \Delta E - \Omega_a\sigma$, where $\Omega_a = Lhb$ is an activation volume. If ΔE is close to k_BT, the dislocation can jump backwards the obstacle, which cancels the previous jump in the "good" direction. During this process, the activation energy is $U^- = \Delta E + \Omega_a\sigma$. As a consequence, the dislocations jumps in the "good" direction with the frequency $\nu_0 e^{-U^+}$ and in the "bad" direction with the frequency $\nu_0 e^{-U^-}$, where ν_0 is an attempt frequency to determine. The average frequency with which the dislocation jumps the barrier in the "good" direction is thus

$$\nu = \nu_0\left(e^{-U^+} - e^{-U^-}\right) = 2\nu_0 e^{-\Delta E/k_BT}\sinh(\Omega_a\sigma/k_BT). \tag{11}$$

The average velocity v of a dislocation is obtained by noting that it moves a distance $L^2/D = L$ (by assuming $L = D$) each time it jumps an obstacle (for a demonstration of this result, see ref. [27]). The resulting velocity is

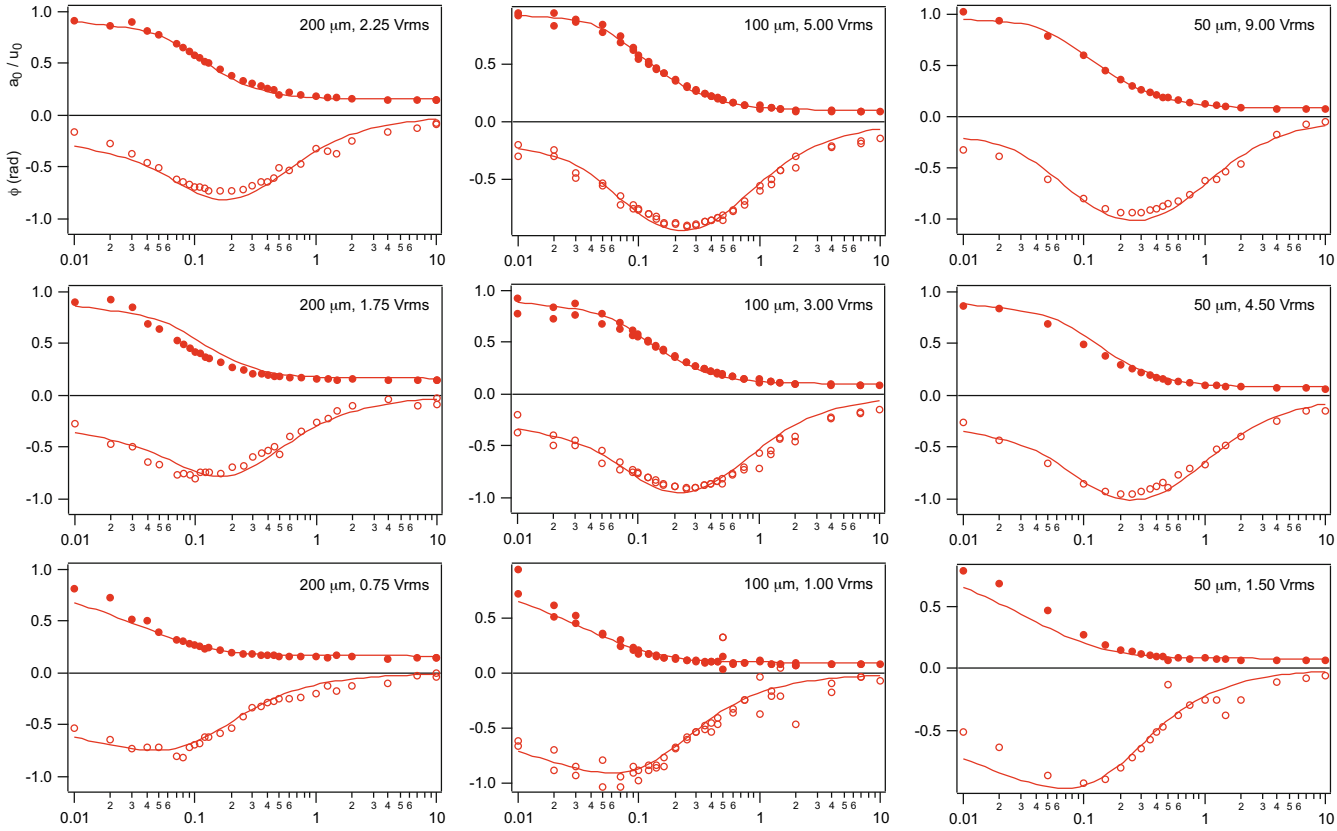

Fig. 7. Ratio a_0/u_0 and phase shift Φ as a function of frequency f. The sample thickness (in μm) and the voltage applied to the ceramics (in Vrms) are given in the upper right corner of each graph (with $u_0 \approx 20\,\text{nm}$ for $V = 1\,\text{Vrms}$). The solid lines have been numerically calculated from our theoretical model with the screw dislocations (see sect. 4.3) by taking $A = 0.16\,\text{dyn/cm}^2$ and $\Omega_a = 2\ 10^{-16}\,\text{cm}^3$ at $d = 50\,\mu\text{m}$, $A = 0.25\,\text{dyn/cm}^2$ and $\Omega_a = 3.1\ 10^{-16}\,\text{cm}^3$ at $d = 100\,\mu\text{m}$ and $A = 0.38\,\text{dyn/cm}^2$ and $\Omega_a = 4.8\ 10^{-16}\,\text{cm}^3$ at $d = 200\,\mu\text{m}$. The best fits of the experimental curves with eqs. (9) of the simplified model are not shown but are very similar to the curves in solid lines visible here.

thus

$$v = \frac{L}{t_{jump} + t_{climb}}, \tag{12}$$

where $t_{jump} = 1/\nu$ is the time the dislocation takes to jump an obstacle and $t_{climb} = L/(m\sigma)$ the time it needs to travel the distance L. Finally, this model predicts that the dislocation moves with a velocity $v = m_{eff}\sigma$ where m_{eff} is a stress-dependent equivalent mobility of the form

$$m_{eff} = \frac{m}{1 + A\frac{\sigma}{\sinh(\sigma\Omega_a/k_BT)}}, \tag{13}$$

where $A = (2m/\nu_0 L)e^{\Delta E/k_BT}$.

The last step is to determine the attempt frequency ν_0. In metallurgy, this frequency is taken as the natural vibration frequency of a dislocation segment of length L pinned at its two ends. By assuming that the segment is along the y-axis, this frequency is obtained by solving the motion equation

$$M\frac{\partial^2 x}{\partial t^2} + \frac{b}{m}\frac{\partial x}{\partial t} - E\frac{\partial^2 x}{\partial y^2} = \sigma b, \tag{14}$$

where $x(y)$ is the displacement of the segment along the x-direction (fig. 9). In this equation, M is the mass of the dislocation per unit length (of the order of ρb^2, where ρ is the mass density [29]) and E is its line tension, equal to the line energy for an edge dislocation (of the order of Bb^2). From this equation, we can construct two quantities: the frequency $\nu_L = \frac{1}{2L}\sqrt{\frac{E}{M}} \sim \frac{1}{2L}\sqrt{\frac{B}{\rho}}$ which would be the natural vibration frequency of the segment in the absence of friction and the relaxation rate $1/\tau_{diss} = b/mM \sim 1/m\rho b$, very large in our system because the climb process is highly dissipative. In practice, $1/\tau_{diss} \gg \nu_L$ which means that the dislocation dynamics is always overdamped. As a consequence the mass term in the l.h.s of eq. (14) can be neglected, which leads to the simplified equation

$$\frac{\partial \bar{x}}{\partial \bar{t}} - \frac{\partial^2 \bar{x}}{\partial \bar{y}^2} = \bar{\sigma} \tag{15}$$

by taking $\bar{x} = x/L$, $\bar{y} = y/b$, $\bar{t} = t/\tau_b$ with $\tau_b = \frac{bL^2}{mE}$ and $\bar{\sigma} = \sigma bL/E$. Solving this equation with the boundary conditions $\bar{x}(0,\bar{y}) = 0$, $\bar{x}(\bar{t},0) = 0$ and $\bar{x}(\bar{t},1) = 0$ yields

$$\bar{x}(\bar{t},\bar{y}) = \sum_{n\,\text{odd}} \frac{4}{\pi^3 n^3}\bar{\sigma}\left(1 - e^{\pi^2 n^2 \bar{t}}\right)\sin(n\pi\bar{y}). \tag{16}$$

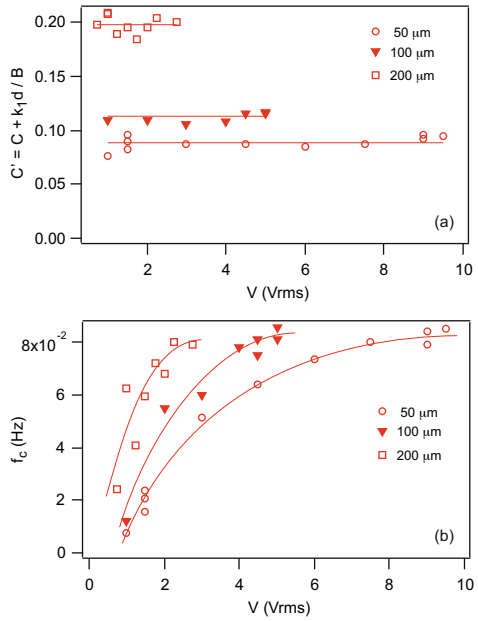

Fig. 8. Constant C' and relaxation frequency f_c obtained from the fit of the rheological curves with eqs. (9) of the simplified model as a function of the voltage V applied to the ceramics (with $u_0 \approx 20\,\text{nm}$ for $V = 1\,\text{Vrms}$). The solid lines are just guides for the eye.

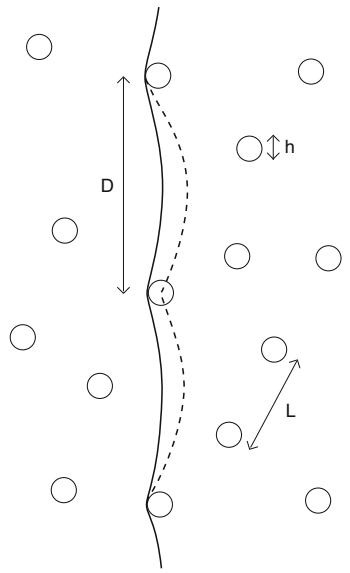

Fig. 9. A dislocation held up by three obstacles separated by distance D moves a distance $h/2$ and sweeps a surface area hD during the activation process when it cuts through one of them.

This equation shows that the typical viscous time for the dislocation to bend under the action of the external stress is τ_b/π^2. As a consequence, and by analogy with the Kramers problem of the Brownian motion of a colloidal particle in a field of force in the large viscosity regime [30], we propose to take $\nu_0 = \pi^2/\tau_b = \frac{\pi^2 mE}{bL^2}$ as a typical attempt frequency in our system.

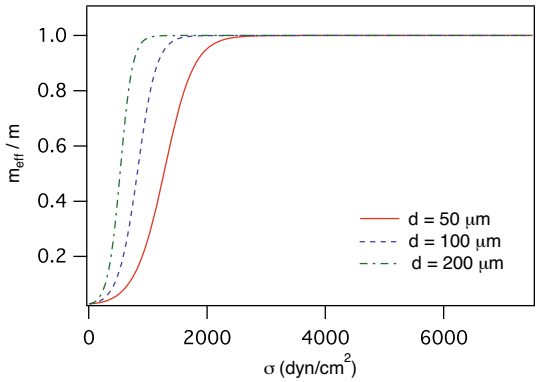

Fig. 10. Ratio of the effective mobility over the intrinsic mobility as a function of the stress for the three thicknesses studied experimentally.

We can fit now our experimental curves of fig. 6 by using the new expression of the mobility given in eq. (13).

4.3 Fit of the experimental curves

To fit our experimental curves, we first need to solve the master equation (8) in which m has been replaced by m_{eff}. This equation can no longer be solved analytically because m_{eff} depends nonlinearly on $\sigma = k_1(u-a)$. On the other hand, this equation can be easily solved numerically by using Mathematica by taking $u(t) = u_0 \sin(\omega t)$ and by setting $a(0) = 0$ as an initial condition. Once the solution $a(t)$ is found numerically, we need to calculate the ratio a_0/u_0 and the phase shift Φ of the first harmonic of $a(t)$ in the stationary regime (this is what we measure experimentally with the lock-in amplifier). This is done numerically by first calculating in the stationary regime the X and Y components of the first harmonic of our signal given by

$$\begin{cases} X = 2\langle \cos(\omega t) a(t) \rangle, \\ Y = 2\langle \sin(\omega t) a(t) \rangle. \end{cases} \tag{17}$$

where the $\langle \ldots \rangle$ denotes a time average. The ratio a_0/u_0 and the phase shift Φ are then calculated from the formula

$$\begin{cases} \dfrac{a_0}{u_0} = \dfrac{\sqrt{X^2+Y^2}}{u_0}, \\ \Phi = \arctan\left(\dfrac{Y}{X}\right). \end{cases} \tag{18}$$

Doing this, we were able to fit our experimental data (solid lines in fig. 7) by taking $A = 0.16\,\text{cm}^2/\text{dyn}$ and $\Omega_a = 2\ 10^{-16}\,\text{cm}^3$ at $d = 50\,\mu\text{m}$, $A = 0.25\,\text{cm}^2/\text{dyn}$ and $\Omega_a = 3.1\ 10^{-16}\,\text{cm}^3$ at $d = 100\,\mu\text{m}$ and $A = 0.38\,\text{cm}^2/\text{dyn}$ and $\Omega_a = 4.8\ 10^{-16}\,\text{cm}^3$ at $d = 200\,\mu\text{m}$. We emphasize that for a reason given later, the fits were done by imposing the constraint that the ratio A/Ω_a is independent of the thickness. The curves of effective mobility m_{eff} corresponding to these values are shown in fig. 10 as a function

of the applied stress. As we can see the mobility strongly decreases below a typical stress that itself decreases when the sample thickness increases. This typical stress is of the order of $1200\,\mathrm{dyn/cm^2}$ at $d = 50\,\mu\mathrm{m}$, $750\,\mathrm{dyn/cm^2}$ at $100\,\mu\mathrm{m}$ and $500\,\mathrm{dyn/cm^2}$ at $d = 200\,\mu\mathrm{m}$. These values roughly correspond to a compression of the sample close to half a layer. This typical value of the applied stress below which the samples become much harder was already mentioned in our old creep experiments performed at constant stress [31,32]. On the other hand, our interpretation of the hardening is now different as we explain in the next subsection.

4.4 On the internal stress and the nature of the obstacles

In our previous works [31,32], we suggested that the hardening of our samples at small stress was due to a pinning of the dislocations in the internal stress field due to the roughness of the glass plates.

To test this assumption, we imaged the surface of our silanized glass plates by AFM (atomic force microscopy) (fig. 11). We observed that, at the micrometer scale, their roughness is close to nm. On the other hand, their surface is also scratched with an average distance between the scratches of a few micrometers for a depth of a few nm. There are also small dust particles (silane grains?) on the surfaces of typical diameter $0.2\,\mu\mathrm{m}$ and height 4–10 nm as the one visible in the figure. The average distance between them is typically 20–50 $\mu\mathrm{m}$. These surface defects, or islands, also generate stresses in the sample.

To estimate the importance of the roughness of the plates, we suppose that the surface at $z = 0$ imposes the layer displacement $u(z = 0) = u_0 \sin(qx) \sin(qy)$. This creates an internal stress in the sample of amplitude in the middle of the sample (at $z = d/2$ and by neglecting the presence of the opposite plate):

$$\sigma_i = 2B\lambda q^2 u_0 \exp(-\lambda q^2 d). \tag{19}$$

By taking for typical values $\Lambda = 2\pi/q = 5\,\mu\mathrm{m}$ and $u_0 = 2\,\mathrm{nm}$, we calculate $\sigma_i \sim 300\,\mathrm{dyn/cm^2}$ in a sample of thickness $d = 50\,\mu\mathrm{m}$. This stress corresponds to a compression of the sample of the order of $b/10$ which is quite small. This stress is still smaller at larger thickness because of its exponential decrease with the thickness. The question now is to determine whether this stress can block the dislocations. This is the case only if the dislocations can bend at a scale of the order of Λ, *i.e.* if E/Λ is smaller than $\sigma_i b$ which imposes $\Lambda > E/\sigma_i b \sim Bb/\sigma_i$. With the value of σ_i given before, this gives $\Lambda > 500\,\mu\mathrm{m}$, which is much larger than the value of Λ taken to calculate σ_i. That means that the dislocations cannot bend (this would cost too much energy) and, consequently, do not interact with σ_i. In conclusion, the internal stress due to the roughness of the glass plates cannot pin the dislocations and can be disregarded.

We now return to the localized obstacles. Two types of objects could act as an obstacle.

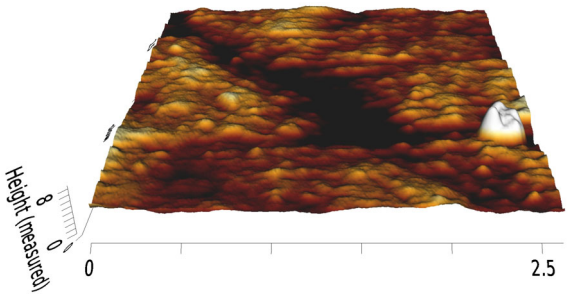

Fig. 11. Typical topography of the surface of the silanized glass plates obtained by contact mode atomic force microscopy. A scratch (along the diagonal) and an isolated dust (which resembles a tooth) are clearly visible. The height is given in nm and the horizontal scale in μm.

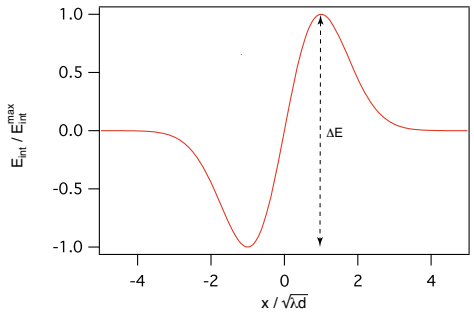

Fig. 12. Interaction energy between a dust particle on a plate and a dislocation in the middle of the sample as a function of their distance along the x-axis perpendicular to the dislocation. The distance x is given in units of $\sqrt{\lambda d}$ and the interaction energy in units of E_{int}^{max}.

The first ones are localized defects on the surfaces such as microscopic holes or small dust particles which are sticked on the surfaces. One example is shown in fig. 11. From an elastic point of view, this object (here an island) can be seen as a small dislocations loop. The interaction energy with an edge dislocation situated in the middle of the sample (at $z = d/2$) has been calculated by Lejček [33] and reads

$$E_{int} = E_{int}^{max} \sqrt{e} \frac{x}{\sqrt{\lambda d}} e^{-\frac{x^2}{2\lambda d}} \tag{20}$$

with $E_{int}^{max} \approx \frac{BbH\delta A}{\sqrt{2\pi} ed}$. In this calculation, the island is at the origin of the coordinates, H is the height of the island, δA is its surface area and x is the distance between the dislocation and the island along the axis perpendicular to the line. At zero stress, the energy necessary to cross the obstacle is (fig. 12)

$$\Delta E = 2E_{int}^{max} \approx \sqrt{\frac{2}{\pi e}} \frac{BbH\delta A}{d}\,. \tag{21}$$

This activation energy is inversely proportional to the thickness. For this reason, the thicker the sample, the easier should be the crossing, which is qualitatively observed. By taking typically $H = 5\,\mathrm{nm}$ and $\delta A = \pi R^2$ with $R = 0.1\,\mu\mathrm{m}$, we calculate $\Delta E \approx 5.4 k_B T$ at $d = 50\,\mu\mathrm{m}$ and $\Delta E \approx 1.3 k_B T$ at $d = 200\,\mu\mathrm{m}$. In order to determine whether these obstacles can be responsible for our

observations, let us calculate the coefficients A and Ω_a of the model for a sample of thickness $d = 50\,\mu$m. Experimentally, we observed that $L \sim 20\,\mu$m (or larger). For these obstacles, $h = 4\sqrt{\lambda d}$ (fig. 12) which gives $h = 9\ 10^{-5}\,$cm at $d = 50\,\mu$m. With these values and by taking $E/b \approx 1\,$dyn/cm [26], we calculate $A \sim 0.1\,\text{cm}^2/\text{dyn}$ and $\Omega_a \sim 5\ 10^{-14}\,\text{cm}^3$. This value of A is similar to the experimental one (0.16), but the activation volume is 200 times larger than the measured one ($2.7\ 10^{-16}\,\text{cm}^3$). As a consequence, the obstacles should be spaced by much less than $1\,\mu$m for the model to match with the experiments, which is impossible. The disagreement is still larger at larger thickness. For these reasons, this explanation must be discarded.

We now consider the role of screw dislocations. These defects are known to be very numerous in smectics [8–12, 15,16,32]. Because a kink is produced on the edge dislocation each time it intersects a screw dislocation, the screw dislocations can be seen as natural obstacles to the propagation of the edge dislocations. This hypothesis was already proposed by Lelidis, Blanc and coworkers [12,17–19] to explain the cusps they observe on the edge dislocations at the AC transition and the jerky motion of the dislocations under compression at small stress. Another reason for this pinning is the presence of a short-range elastic force F_{int} between the two types of dislocations when they are very close to each other. This force was calculated by Lelidis *et al.* [12] in nonlinear elasticity by taking into account the anharmonic correction in the expression of the elastic energy [1]. According to their calculation, $F_{int} \sim 2.5\ 10^{-7}\,$dyn (2.5 pN) when the dislocations are a distance b apart by taking $B = 5\ 10^7\,\text{erg/cm}^3$. To determine whether the crossing with the screw dislocations can explain our rheological curves in 8CB, let us estimate the constant A and the activation volume Ω_a of the model. Because the obstacles are screw dislocations, L is the mean distance between the screw dislocations and $h \sim b$, so that

$$A = \frac{2}{\pi^2}\frac{bL}{E}e^{\Delta E/k_BT} \quad \text{and} \quad \Omega_a = Lb^2. \tag{22}$$

In addition, the activation energy ΔE must be independent of the thickness because the crossing is a local process. As a consequence, this model predicts that A/Ω_a is also independent of the thickness since it does not depend on L, an assumption we made to fit our experimental data and obtain the values of A and Ω_a given above. From these values and eq. (22), we can now calculate L and ΔE on condition that we know the Burgers vector of the dislocations.

Let us first assume that all the dislocations are elementary. In this case, $b \approx 3\,$nm and we obtain $L = 22\,\mu$m at $d = 50\,\mu$m, $L = 34\,\mu$m at $d = 100\,\mu$m and $L = 54\,\mu$m at $d = 200\,\mu$m and $\Delta E = 0.15\,\text{eV} = 5.9\,k_BT$ knowing that $E/b \approx 1\,$dyn/cm at 32 °C [26]. In theory, ΔE must be of the order of $F_{int}b$ or comparable to the energy of the kink created on the edge dislocation. For elementary dislocations, $F_{int}b \sim 7.5\ 10^{-14}\,\text{erg} = 2k_BT$. As for the kink energy E_{kink}, it must be of the order of $E_{screw}b$ knowing that the kink is of a screw character. In a smectic-A LC, the energy of a screw dislocation reduces to its core energy which was found to be of the order of $0.1Bb^2$ for an elementary dislocation. This value was deduced from the measurement of critical stress above which the helical instability develops [15] (in 8CB, this critical stress is larger than σ_c). By taking this value, we calculate $E_{kink} \sim 0.1Bb^3 = 3k_BT$. These two estimates are typically twice as small as the experimental value. This could be due to the approximations made in the model, in particular in the calculation of ν_0. This being, we should increase ν_0 by more than a factor of 10 to decrease the experimental value of ΔE by a factor of 2, which seems quite excessive.

A more likely explanation is that the dislocations are not elementary. This would be surprising for the screw dislocations because their energy (out of the core) is proportional to b^2 (by assuming that their core radius is of the order of b). This strongly favors elementary screw dislocations as confirmed by direct TEM observations [34]. The situation is different for the edge dislocations because their energy is proportional to b [1, 26, 35]. Because of this property, these dislocations tend to group together when the angle α is "large", as in our experiment ($\alpha = 10^{-3}\,$rad) [1, 2]. It is thus very likely that the edge dislocations pair up to form dislocations of Burgers vector $b = 2b_0$. With this new assumption, we calculate $L = 11\,\mu$m at $d = 50\,\mu$m, $L = 17\,\mu$m at $d = 100\,\mu$m and $L = 27\,\mu$m at $d = 200\,\mu$m and $\Delta E = 0.15\,\text{eV} = 6.6\,k_BT$ knowing that E/b remains unchanged as shown experimentally in [26]. As we can see the value found of ΔE is almost the same. On the other hand, we predict an activation energy twice as large as before because F_{int} is proportional to b, which agrees much better with experiments. For this reason, we think that our dislocations are of Burgers vector $b = 2b_0$.

To conclude this discussion, let us verify that our working assumption $D \approx L$ is correct. According to Friedel [27], the distance D must be larger than L at small stress and given by formula

$$D = \left[\frac{2EL^2}{\sigma b}\right]^{1/3}. \tag{23}$$

In our experiments at $d = 50\,\mu$m, σ varies typically between 1500 and $7000\,\text{dyn/cm}^2$ which gives $7\,\mu\text{m} < D < 12\,\mu\text{m}$ by taking $L = 11\,\mu$m. As we can see these values of D are comparable or smaller than L which is impossible. This means that we are not in the Friedel regime but rather in a regime of large stress in which $L \approx D$ as was shown numerically in ref. [28]. One easily checks that the same conclusion holds at thicknesses $d = 100$ and $200\,\mu$m with the values of L given above. This proves the validity of our model for the typical stresses used in our experiment.

Another consequence of this discussion is that the mobility m here measured certainly corresponds to the mobility of edge dislocations of Burgers vector $b = 2b_0$. As recalled in sect. 3, the value found is in excellent agreement with the value found at smaller angle for elementary edge dislocations. This observation proves that the mobil-

ity is the same for dislocations of Burgers vector $b = b_0$ and $b = 2b_0$. This result, already stressed in refs. [31,32], was confirmed by direct measurements in free-standing films of the mobility of dislocations of Burgers vector $b = 2b_0$ [36] and agrees with the predictions of the hydrodynamic model which predicts that m must be independent of b [1,37].

As for the distance between the screw dislocations, it quite well agrees with the usual values found in the literature. An interesting point here is that the density of screw dislocations L^{-2} decreases more or less as $1/d$ when the thickness increases.

From this discussion, we conclude that the edge dislocations are probably of Burgers vector $b = 2b_0$ when $\alpha = 10^{-3}$ rad and that the decrease of their mobility at small stress is due to their thermally activated crossing with elementary screw dislocations.

In the next subsection, we test these conclusions by repeating the same experiments at a smaller angle, when the dislocations are elementary. In this case, ΔE must be smaller, typically twice as small. For this reason, the crossing with the screw dislocations must be easier and the sample hardening at low stress must be less important.

4.5 Final test of the model when the dislocations are elementary

We performed new experiments at $d = 100\,\mu$m and $\alpha = 5\ 10^{-4}$ rad. At this angle, the dislocations are elementary [5]. To test our theoretical predictions, we measured again the rheological curves at voltages 5, 3 and 1 Vrms (corresponding to $u_0 = 100, 60$ and 20 nm, respectively) and we calculated the corresponding curves predicted by the model. The same values of the parameters as the ones measured previously at $d = 100\,\mu$m were used, except for ω_c and ΔE that were divided by 2 to account the fact that α and b are twice as small. Note that, in doing so, we assume that the density of screw dislocations depends only on the thickness. The curves calculated in this manner (solid lines in fig. 13) are in very good agreement with the experimental curves. By contrast, the curves calculated by keeping the same value of ΔE significantly shift from the experimental ones at low voltages, as we can see in fig. 13(b), (c). This provides compelling evidence that the crossing between edge and screw dislocations is more difficult at $\alpha = 10^{-3}$ rad than at $\alpha = 5\ 10^{-4}$ rad, which we interpret as due to the probable formation of double dislocations of Burgers vector $b = 2b_0$. For completeness, we show in fig. 14 the shape of the effective mobility curves predicted for the two types of dislocations, elementary and double.

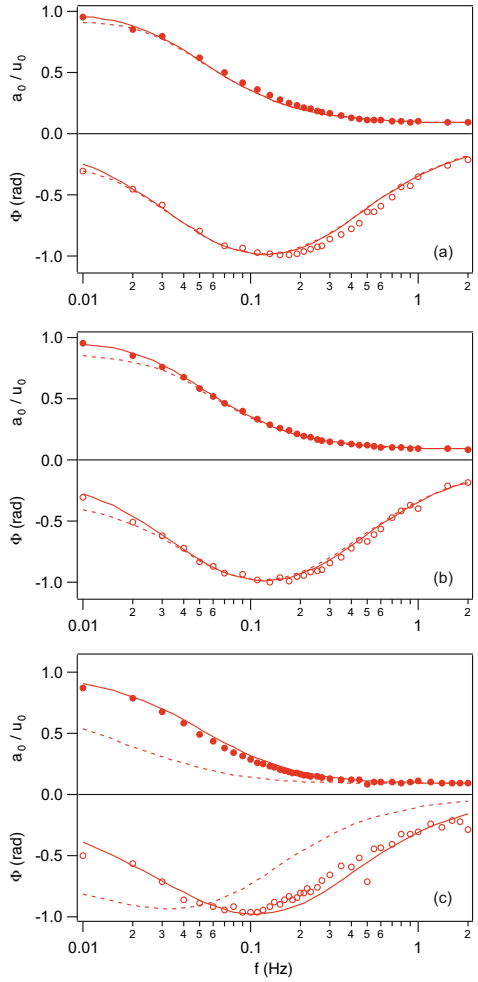

Fig. 13. (a)–(c) Rheological curves when $d = 100\,\mu$m and $\alpha = 5\ 10^{-4}$ rad. (a) $V = 5$ Vrms ($u_0 = 100$ nm); (b) $V = 3$ Vrms ($u_0 = 60$ nm); (c) $V = 1$ Vrms ($u_0 = 20$ nm). The curves in solid (dashed) lines have been calculated from the model by taking $\omega_c = 0.255$ Hz and $\Delta E = 3.3 k_B T$ ($6.6 k_B T$).

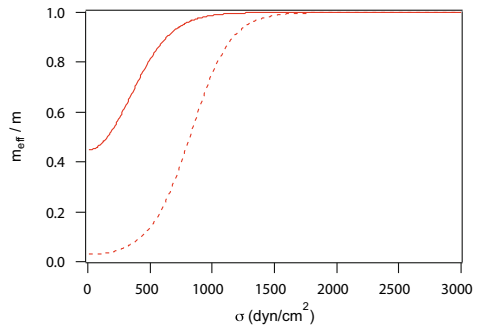

Fig. 14. Effective mobility of the edge dislocations predicted by the model at $d = 100\,\mu$m. The curve in solid (dashed) line, calculated by taking $\Delta E = 3.3 k_B T$ ($6.6 k_B T$), corresponds to elementary (double) dislocations.

5 Conclusions

We have revisited the model of creep by climb of edge dislocations in a homeotropic sample of smectic-A LC. Our measurements show that the samples are more viscous at low stress than at large one, in disagreement with the standard model. This nonlinear effect can be explained by introducing a mobility effective for the dislocations which decreases at low applied stress. This decrease is attributed

to the crossing with the screw dislocations which are numerous in the samples. A fine analysis of the rheological data shows that this effect depends on the angle between the plates because of a tendency of the dislocations to pair up when the angle increases. Of course, it would be important to check this point more directly, for instance by visualizing the dislocations under the microscope thanks to the introduction of nanoparticles.

It would also be important in the future to understand why the interaction between the edge and screw dislocations is stronger at the AC phase transition, where a clear yield stress is observed, even in thick samples. This is surprising because B, and consequently the activation energy ΔE, are expected to decrease at this transition, which should favor the crossing between the dislocations.

It would also be interesting to test what happens in very thin samples as the ones studied by Herke *et al.* in a force machine in the sphere-plane geometry. In their experiments with 8CB, these authors mention a large yield stress. In our opinion, this stress could come from the internal stress generated by some defects on the surfaces in the central part of the sample and from the interactions between the screw dislocations and the giant edge dislocations that should form in the external part of the sample because of the geometry.

Finally, it would also be important to understand why the density of screw dislocations decreases when the sample thickness increases, remembering that in our experiments all measurements were conducted with the same glass plates and the same surface treatment. We note at this point that the same tendency was also observed by Blanc in his samples at the AC phase transition [38].

PO warmly thanks Vincent Dolique for his help with the AFM measurements and A. Naert and S. Ciliberto for useful discussions about stochastic phenomena. F. Bunel, A. Dequidt and E. Kats are also thanked for their critical reading of the manuscript.

Author contribution statement

PO performed the experiments, proposed the model used to fit the data and wrote the paper. GP wrote the driver for the RKC temperature controllers and the Labview program used to control the rheometer.

References

1. P. Oswald, P. Pieranski, *Smectic and Columnar Liquid Crystals: Concepts and Physical Properties Illustrated by Experiments* (Taylor & Francis, CRC Press, Boca Raton, 2006).
2. R. Bartolino, G. Durand, Phys. Rev. Lett. **39**, 1346 (1977).
3. R.B. Meyer, B. Stebler, S.T. Lagerwall, Phys. Rev. Lett. **41**, 1393 (1978).
4. J. Milette, V. Toader, L. Reven, R.B. Lennox, J. Mater. Chem. **21**, 9043 (2011).
5. P. Oswald, J. Milette, S. Relaix, L. Reven, A. Dequidt, L. Lejček, EPL **103**, 46004 (2013).
6. P. Oswald, L. Lejček, Eur. Phys. J. E **40**, 84 (2017).
7. M. Kléman, Philos. Mag. **34**, 79 (1976).
8. L. Bourdon, *Contribution à l'étude des défauts dans les phases smectiques à couches liquides*, M.Sc. Thesis, University of Paris XI, Orsay, 1980.
9. K. Ishikawa, T. Uemura, H. Takezoe, A. Fukuda, Jpn. J. Appl. Phys. **23**, L666 (1984).
10. M. Kléman, C.E. Williams, J.M. Costello, T. Gulik-Krzywicki, Philos. Mag. **35**, 33 (1977).
11. M. Allain, Europhys. Lett. **2**, 597 (1986).
12. I. Lelidis, C. Blanc, M. Kléman, Phys. Rev. E **74**, 051710 (2006).
13. P. Oswald, D. Lefur, C.R. Acad. Sci. Paris, Série II **297**, 699 (1983).
14. L. Bourdon, M. Kléman, L. Lejček, D. Taupin, J. Phys. (Paris) **42**, 261 (1981).
15. P. Oswald, M. Kléman, J. Phys. (Paris) Lett. **45**, L319 (1984).
16. R.A. Herke, N.A. Clark, M.A. Handschy, Phys. Rev. E **56**, 3028 (1997).
17. I. Lelidis, M. Kléman, J.L. Martin, Mol. Cryst. Liq. Cryst. Sci. Technol., Sect. A **330**, 457 (1999).
18. I. Lelidis, M. Kléman, J.L. Martin, Mol. Cryst. Liq. Cryst. Sci. Technol., Sect. A **351**, 187 (2000).
19. C. Blanc, N. Zuodar, I. Lelidis, M. Kléman, J.L. Martin, Phys. Rev. E **69**, 011705 (2004).
20. P. Oswald, Phys. Rev. E **92**, 062508 (2005). Note here that a factor of 2 is missing in the denominator of eq. (37) of this paper.
21. R. Ribotta, G. Durand, J. Phys. (Paris) **38**, 179 (1977).
22. N.A. Clark, A.J. Hurd, J. Phys. (Paris) **43**, 1159 (1982).
23. J.C. Géminard, R. Holyst, P. Oswald, Phys. Rev. Lett. **78**, 1924 (1997).
24. F. Picano, R. Holyst, P. Oswald, Phys. Rev. E **62**, 3747 (2000).
25. P. Oswald, F. Picano, F. Caillier, Phys. Rev. E **68**, 061701 (2003).
26. A. Żywociński, F. Picano, P. Oswald, J.C. Géminard, Phys. Rev. E **62**, 8133 (2000).
27. J. Friedel, *Dislocations* (Pergamon Press, New York, 1967) p. 224.
28. A.J.E. Foreman, M.J. Makin, Philos. Mag. **14**, 911 (1966).
29. F.R.N. Nabarro, *Theory of Crystal Dislocations* (Dover, New York, 1987).
30. H.A. Kramers, Physica (Utrecht) **7**, 284 (1940).
31. P. Oswald, C.R. Acad. Sci. Paris, Série II **296**, 1385 (1983).
32. P. Oswald, *Dynamique des dislocations dans les smectiques A et B*, D.Sc. Thesis, University of Paris XI, Orsay, 1985.
33. L. Lejček, Liq. Cryst. **1**, 473 (1986).
34. C. Zhang, O.D. Lavrentovich, A. Jàkli, Proc. SPIE **9769**, 97690D-1 (2016).
35. M. Kléman, J. Phys. (Paris) **35**, 595 (1974).
36. P.V. Dolganov, E.I. Kats, V.K. Dolganov, JETP Lett. **106**, 229 (2017).
37. E. Dubois-Violette, E. Guazzelli, J. Prost, Philos. Mag. **48**, 727 (1983).
38. C. Blanc, private communication.